



Optical Resonator Based Biomolecular Sensors and Logic Devices

Frank Vollmer¹ and Sukhdev Roy²

Abstract | Optical resonator based biosensors are emerging as one of the most sensitive microsystem biodetection technology that boasts all of the capabilities for a next-generation lab-on-chip device: label-free detection down to single molecules, operation in aqueous environment and cost-effective integration on microchips together with other photonic, electronic and fluidic components. We give a scholarly introduction to the emerging field of optical resonator based biosensing, review current applications, and explain how optical resonators are coated with biomolecules to construct logic devices.

1 Nano-Biotechnology: Sensors Interface the Molecular World

The ability to synthesize and fabricate devices with micro-to nanoscale precision has revolutionized biotechnology and spawned the new field of nanobiotechnology. Fabrication of miniature **biosensor** elements is particularly important since the increase in surface to volume ratio of the micro-to nanoscale devices can dramatically boost sensitivity levels, for example of mechanical,^{1–2} electrical^{3–4}, photonic and plasmonic^{5–7} biosensors. This unprecedented detection capability of nanobiotechnology-enabled sensors is not only revolutionizing clinical diagnostics⁸ but is also opening the door for detailed explorations of the molecular world, the world of bioparticles, single molecules, molecular machines, and their interactions⁹. In fact the development of some of these nanobiotechnology-based biosensors has already enabled detection down to single **virus** particles and even single molecules.^{3,5,10–11}

For all of the proposed biosensing applications, it is most important to achieve highly sensitive detection capability in *aqueous* solution since most biological and clinical samples are water-based. Furthermore, **biomolecules** mostly function in aqueous environments and also clinical diagnostic assays rely on specific molecular recognition *in solution*. It is equally important to achieve sensitive detection *in real-time*, *without the need for labels*, on fully automated chip-scale devices. Optical resonator biosensors, also

called **optical microcavities**, have emerged as one of the most sensitive micro-/nanosystems biodetection technology that boasts all of the desired capabilities: label-free detection, potential single molecule sensitivity, operation in aqueous environment and cost-effective integration on microchips together with other photonic, electronic and fluidic components.¹² Figure 1 and Table 1 compare optical resonator biosensors with other nanobiotechnology-enabled sensors that have been developed for label-free single virus detection. As we will review in the following, optical resonators are not only being developed as sensors that probe the biological world but also as a platform to construct all-optical switches and logic devices by leveraging the astounding optical properties found in biomolecules.

2 Optical Resonator Biosensors

2.1 Label-free biosensor technology

Perhaps the simplest example for an optical resonator is a glass microsphere, about 100 μm in diameter, which is used to trap a light ray by total internal reflection (TIR). TIR is a well known optical effect that is observed for light reflected at the surface of a glass prism, if the incident angle θ is larger than the critical angle $\theta_c = \arcsin(n_{\text{air}}/n_{\text{glass}})$, see Figure 2. For the case of the microsphere, multiple TIRs guide the light around the sphere's circumference so that the returning light wave starts to interfere with itself. Light can only remain confined on this trajectory

Biosensor: A biosensor is an analytical device that transduces a molecular binding event into a detectable optical or electrical signal.

Virus: A virus is an infectious bioparticle in the ~20–500 nm size range that spreads outside of cells but requires the cell to replicate.

Biomolecule: A biomolecule is synthesized by cells or bacteria. The synthesis of biomolecules from naturally occurring pre-cursor molecules such as aminoacids or nucleotides is directly or indirectly encoded by a genetic blueprint. Changes in the genetic blueprint for example by random mutations enable the evolution of new and improved biomolecules which manifest themselves by their coding in specific genes.

¹Max Planck Institute for the Science of Light, Laboratory of Biophotonics & Biosensing, Erlangen, Germany. frank.vollmer@mpl.mpg.de

²Department of Physics and Computer Science, Dayalbagh Educational Institute, Agra, India. sukhdevroy@dei.ac.in

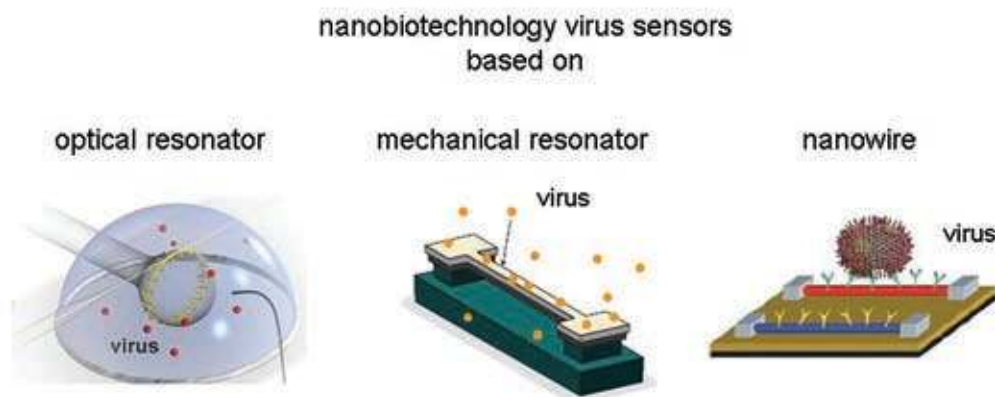


Figure 1: Nanobiotechnology-enabled single virus detectors. From left to right: optical resonator, nanomechanical resonator and nanowire sensor. Adapted from references 10, 11 and 13.

Table 1: Overview of the capabilities of nanobiotechnology-enabled sensors: optical resonator, nanomechanical resonator and nanowire biosensors. MW = molecular weight.

	Optical resonator	Mechanical resonator	Nanowire sensor
Transduction scheme	optical frequency shift ¹²	mechanical frequency shift ¹¹	conductance change ³
Sensitive to	polarizability, proportional to MW ¹⁴	MW ²	charge ³
Operation in water	yes ^{12,15}	limited ¹⁶	yes ¹⁷
Detection by molecular recognition	yes ¹⁸	possible ¹⁶	yes ¹⁷
Single molecule detection capability	possible ¹²	demonstrated in vacuum ¹¹	possible ¹⁹
Single virus detection	demonstrated for Influenza A virus ¹⁰	demonstrated for virus in vacuum ²⁰	demonstrated for Influenza A virus ¹³
Microfluidic integration	yes ²¹	limited ¹⁶	yes ¹⁹
Multiplexing	yes ²²	yes ²	yes ³
Fabrication on chip	bottom-up ²³ as well as top down ²⁴	top-down ²	bottom-up ³
Logic devices	yes ²⁵	yes (in vacuum) ²⁶	yes ²⁷

Optical microcavity: An optical microcavity confines coherent light by total internal reflection which interferes to produce an optical resonance signal. The resonance signal can be identified as a narrow line in the spectral response of the microcavity. Examples for optical microcavities are glass beads, Fabry Perot resonators or ring resonators. Optical microcavities are also referred to as optical resonators.

Nanomechanical resonator biosensor: Nanomechanical resonator biosensors such as silicon nanobeams or silicon cantilevers detect the added weight Δm after binding of a biomolecule or virus particle to the miniature sensor element with resting mass m_0 . The added weight is detected and quantified from the shift $\Delta\omega$ of the mechanical resonance frequency ω which changes upon binding^{11,20} according to

$$\frac{\Delta\omega}{\omega} = -\frac{\Delta m}{2m_0}$$

if the interference is constructive which means that an exact integer number N of wavelengths λ have to fit on the closed optical path. This confined light wave is also known as a ‘whispering gallery mode’ (WGM), since its trajectory resembles that of a sound wave reflected along the Whispering Gallery in St. Paul’s Cathedral in London, see Figure 2.

Light remains confined within the microsphere and recirculates for many tens of thousands of times since the dominant absorption loss in silica glass is only ~ 7 dB/km. Furthermore, the number of total-internal reflections per orbit of a WGM is typically very large (many more than depicted in Figure 2) so that the polygonal optical path resembles more that of a circular optical path circumnavigating close to the microsphere surface

as shown in Figure 3. This simple picture leads us to the approximate WGM resonance condition:

$$N \times \lambda_r / n = 2\pi R \quad (1)$$

which states that N number of wavelengths λ_r have to fit on the circular optical path of length $2\pi R$, with microsphere radius R and microsphere refractive index n . The resonance frequency of the WGM is then calculated as $\omega = 2\pi f = 2\pi \frac{c}{\lambda_r} = \frac{cN}{nR}$.

Similar to a **nanomechanical resonator biosensor**, the miniature optical resonator detects the binding of analyte molecules from changes in the WGM resonance frequency. The binding of a biomolecule will red-shift the resonance frequency by a miniscule amount, see Figure 3. The red shift

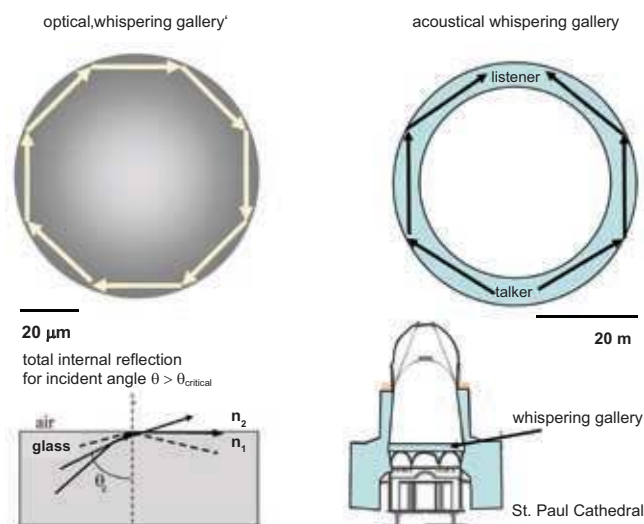


Figure 2: Left: Total-internal reflection of light in a microsphere and at a prism. Right: Acoustic 'Whispering Gallery' in St. Paul's Cathedral, London.

occurs since the bound DNA or protein biomolecule will 'pull' part of the optical field to the outside of the microsphere, effectively increasing the path length by $2\pi\Delta l$. This increase in path length produces a red shift $\Delta\omega$ in resonance frequency ω according to:

$$\frac{\Delta\omega}{\omega} = -\frac{2\pi\Delta l}{2\pi R} = -\frac{\Delta l}{R} \quad (2)$$

Figure 4 shows the first experimental setup that was built to measure the WGM resonance frequency shift upon specific binding of Streptavidin protein molecules from solution.^{23,28} The microsphere resonators that were used in this demonstration were fabricated by simply melting the tip of an **optical fiber** either with a hydrogen torch or a CO_2 laser. In both cases, the glass is heated and softened so that surface tension forms a spherical object sitting on the fiber stem. The fiber stem allows positioning and alignment of the microsphere with respect to an optical fiber that is used to excite the WGM along the microsphere equator, where the orbiting light does not interfere with the stem. This exciting optical fiber is tapered and put in contact with the microsphere to allow for **evanescent coupling**. A continuous-wave near infrared tunable distributed feedback **DFB laser** is coupled into one end of this fiber and used to probe the resonance frequency of the microsphere. As the laser frequency is tuned and matches the resonance frequency of the microsphere, the light evanescently couples into the WGM and no longer transmits to the end of the fiber. A photodetector connected to the fiber end now records a Lorentzian-shaped drop in intensity

for every WGM. This transmission spectrum (Figure 4b) is recorded every millisecond in 'real-time' for each scan of the laser and is stored and analyzed on a computer. Several Lorentzian-shaped drops are observed in the transmission spectrum for one scan of the laser and the minimum of each corresponds to the resonance frequency of one WGM. For the biosensing experiments discussed in the following, it is sufficient to monitor only one of the WGM resonance frequencies.

It has been shown that the binding of Streptavidin molecules to the microsphere from solution will induce a red-shift of the WGM resonance frequency.²³ The shift in resonance frequency is plotted as $\left|\frac{\Delta\omega}{\omega}\right|$ versus time. Such a plot is shown in Figure 4d. The frequency shift signal increases and saturates as Streptavidin molecules occupy all of the binding sites provided by previously surface-immobilized biorecognition elements. In this example, BSA-biotin (bovine serum albumin protein conjugated to biotin) has been used as the specific recognition element for Streptavidin, see Figure 4c. As the frequency shift signal saturates, a complete monolayer of Streptavidin molecules forms on top of the BSA-Biotin layer. At saturation, Streptavidin forms an added optically contiguous layer which exhibits the same refractive index as the glass microsphere ($n \sim 1.45$).²³ The monolayer thus effectively increases the circumference of the glass microsphere by $2\pi \Delta t$ where Δt is the diameter of a Streptavidin molecule with $\sim 2.5 \text{ nm}$ radius of gyration. The frequency shift $\left|\frac{\Delta\omega}{\omega}\right|$ associated with

Optical fiber: A single mode optical fiber is a $\sim 125 \mu\text{m}$ -diameter glass fiber that transmits light by total internal reflection (TIR). The light is guided by TIR through a higher-refractive index glass core ($\sim 6 \mu\text{m}$ core diameter) surrounded by the slightly lower refractive index glass cladding ($\sim 125 \mu\text{m}$ total diameter).

Evanescent coupling: Light that is total internally reflected at the surface of a prism can couple to a symmetrically opposed prism by evanescent coupling if the two prisms are brought in close proximity, so that the distance between the surfaces is on the order of the evanescent field length, typically a fraction of the wavelength or about 100–300 nm for visible light.

DFB Laser: A Distributed Feedback Laser is a laser diode internally modified with a grating structure to produce a narrow laser linewidth $\sim 100 \text{ kHz}$. The center wavelength of a DFB laser can be tuned continuously by changing the laser diode current in the mA range. Wavelength tuning is typically achieved within a range of 0.1–0.3 nm, with a typical tuning coefficient $\sim 0.01 \text{ nm/mA}$. DFB lasers are widely used in the telecommunications industry as inexpensive chip-scale devices.

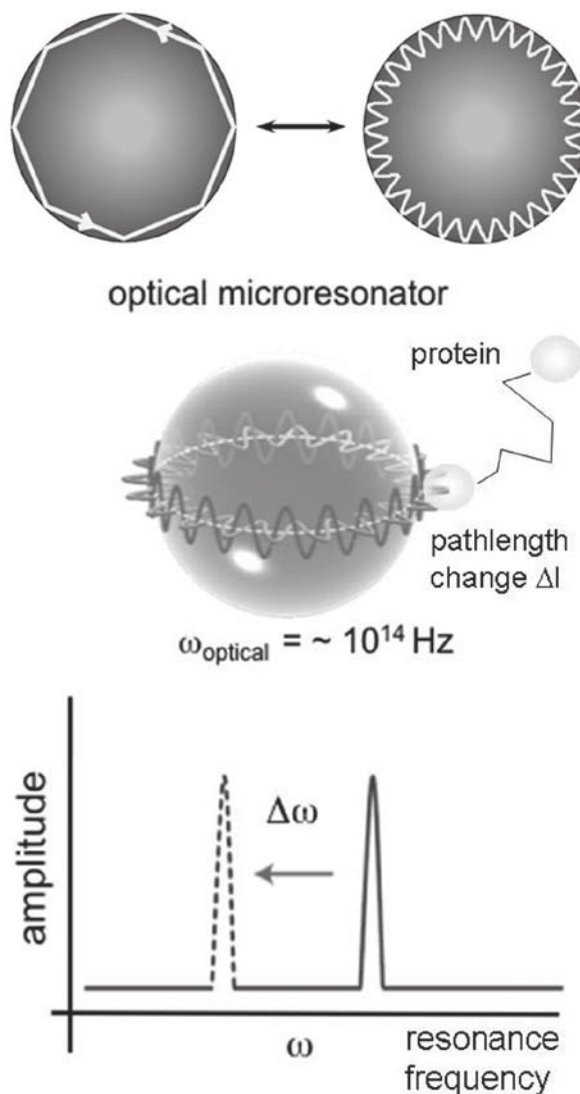


Figure 3: Top: Illustration of the optical resonance called Whispering Gallery Mode (WGM) in a glass microsphere. Bottom: Binding of a protein to the microsphere surface increases the WGM path length and is detected from a resonance frequency shift $\Delta\omega$.

Streptavidin monolayer formation on the microspheres ($R = 150 \mu\text{m}$) is estimated from equation (2):

$$\left| \frac{\Delta\omega}{\omega} \right| = \left| -\frac{\Delta l}{R} \right| = \left| -\frac{2.5 \text{ nm}}{150000 \text{ nm}} \right| = 1.45 \times 10^{-5} \quad (3)$$

which is in good agreement with the measurement presented in Figure 4d.

Detecting the frequency shift associated with monolayer formation is an easy task for our optical resonator biosensor since the WGM line width $\Delta\omega_{\text{line}}$ is much smaller than the frequency shift $\Delta\omega$. The narrow line width of a WGM resonator is associated with the high quality **Q-factor** of the optical resonance. The Q-factor is determined from the line width of the resonance as $Q = \omega/\Delta\omega_{\text{line}}$, about

2×10^6 in this example. In fact, Q-factors of more than 10^7 have been obtained for optical resonators immersed in aqueous environments and ultimate Q's only limited by the absorption in the glass material of up to 10^{10} have been reported in $\sim 100 \mu\text{m}$ glass microspheres in air^{29–30}. A single Streptavidin monolayer shifts the WGM resonance line of a $Q = 10^7$ and $R = 150 \mu\text{m}$ microsphere through 100 line widths, and through about 10^5 line widths for a $Q = 10^{10}$, certainly an easy signal to detect!¹⁰ Because of their large Q-factors optical resonator biosensors surpass the detection limits of commercial label-free biosensors such as quartz crystal microbalances and surface plasmon resonance detectors. The extremely sensitive method for detecting biomolecules from frequency shift measurements in high-Q resonators

Q factor: Q factor is the figure of merit of a resonant system and is inversely proportional to the relative amount of energy $\Delta E/E_{\text{total}}$ that is lost per oscillation: $Q = 2\pi E_{\text{total}}/\Delta E$. For example, the Q-factor of Foucault's Pendulum in the Pantheon in Paris may reach $Q = 1000$, a typical electronic LC circuit filter has a $Q \sim 20$, a nanomechanical system in vacuum may exhibit Q's up to 10^{5-6} and optical resonator biosensors can reach ultimate Q's of up to 10^{10} .

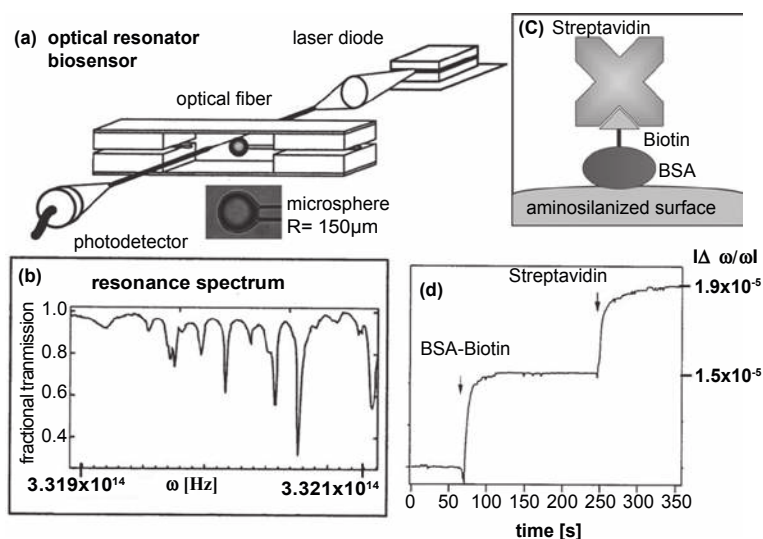


Figure 4: (a) First experimental setup to demonstrate optical resonance WGM frequency shifts for specific detection of a biomolecule called Streptavidin, adapted from reference 23; (b) WGM resonances appear as Lorentzian dips in the fiber-coupled microsphere transmission spectrum; (c) Specific detection of Streptavidin is achieved by molecular recognition through the receptor element BSA-Biotin; (d) Resonance frequency shifts vs time for Streptavidin binding to BSA-biotin, forming monolayer surface coverage at saturation. The arrow indicates the time point at which Streptavidin was added to the liquid sample cell.

Table 2: Examples for optical resonator biosensors that have been utilized or proposed in biosensing applications.

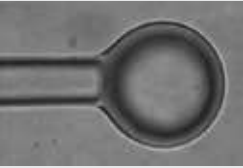
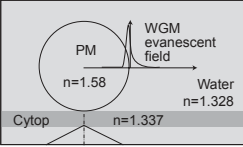
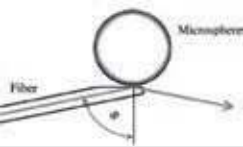

Optical resonator biosensor	Device example	Potential single molecule resolution	Multiplexing capability	Resonator functionalization
Microsphere waveguide coupled ^{5,23,30,39-43}		yes	limited	dip-coating, (hang-drop) ²⁸
Microsphere, prism coupled ³⁷		yes	yes	bulk chemistry, micropatterning
Microsphere, angle polished fiber coupled ^{29,44}		yes	no	no biosensor demonstration yet
Microtoroid, fiber coupled ^{18,31-32,45}		yes	limited	microfluidics, micropatterning

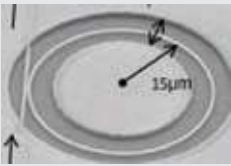

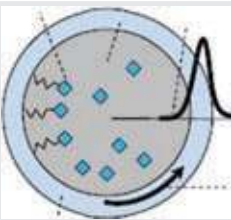
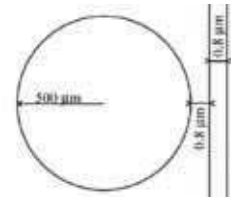

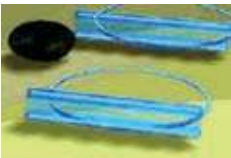
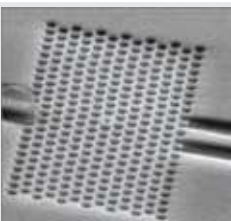
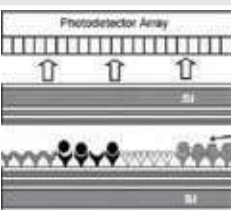
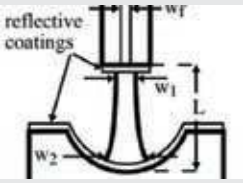


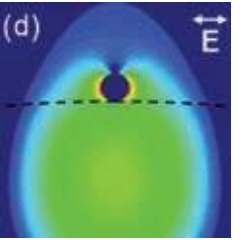
Table 2: (Continued).				
Optical resonator biosensor	Device example	Potential single molecule resolution	Multiplexing capability	Resonator functionalization
Ring resonator, waveguide coupled ^{24,46-50}		not proposed	yes	microfluidics or micropatterning ⁵¹
Fluorescent microsphere ⁵²⁻⁵⁷		no	yes	bulk chemistry
Capillary, fiber coupled (LCORR) ^{33,58}		not proposed	limited	microfluidics
Disk resonator, ^{59,60} waveguide coupled		not proposed	yes	micropatterning, microfluidics
Bottleneck resonator ⁶¹		not proposed	limited	no biosensor demonstration yet
Microtube ring resonators ⁶²		not proposed	yes	microfluidics
Photonic crystal resonator ^{34-36,63-64}		yes	yes	microfluidics or micropatterning
Fabry perot resonator ⁶⁵		not proposed	yes	micropatterning, microfluidics, dip-pen

Table 2: (Continued).

Optical resonator biosensor	Device example	Potential single molecule resolution	Multiplexing capability	Resonator functionalization
Fiber-based ⁶⁶⁻⁶⁷		not proposed	limited	microfluidics, micropatterning
Micro-bubble ⁶⁸⁻⁷⁰		not proposed	limited	microfluidics
Micro-coil ⁷¹⁻⁷³		not proposed	limited	microfluidics
Photonic-plasmonic WGM: microsphere coupled to nanoantenna ⁷⁴⁻⁷⁶		yes	yes	micropatterning, bulk chemistry

has been coined the 'reactive sensing principle'²⁵ since this principle applies to any optical resonator and to any biomolecule. Other examples for high-Q optical resonators are silicon ring resonators,²⁴ toroidal glass resonators,³¹⁻³² hollow glass capillaries³³ and silicon photonic crystal-type resonators.³⁴⁻³⁶ The different geometries and materials have all their unique advantages in biosensing: microspheres are extremely simple to fabricate, exhibit the highest Q and were the first optical resonator that were used in biosensing.^{5,28,37} Silicon ring resonators are micro-fabricated using top-down photolithography combined with reactive ion etching and are easily integrated into larger sensor arrays.²⁴ Hollow-core glass capillaries that confine light along their perimeter, so called liquid core optical ring resonators (LOCRRs), are sensitive to molecules binding to their interior. They are fabricated by pulling thin-walled capillaries and can easily be combined with microfluidics.³⁸

The availability of the many geometries and materials that can be used for label-free biosensing on chip-scale devices makes the optical resonator microsystem biodetection technology particularly attractive for many research groups around the world that have an interest in engineering and in their use as sensitive devices for applications in life sciences, healthcare, point-of-care, environmental monitoring and emergency response.¹² Table 2 gives an overview over the variety of optical resonator biosensors that are being developed.

2.2 The reactive sensing principle

To understand the light-matter interaction of a molecule with the microsphere cavity we have to take a closer look at the perturbation induced by the biomolecule bound at the resonator surface. Once bound to the equator of the microsphere, a Streptavidin protein molecule is exposed to

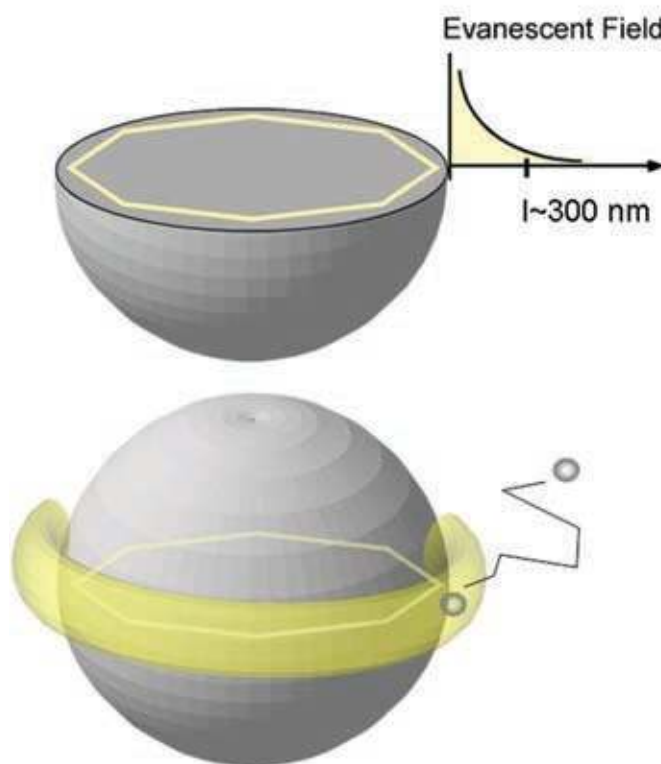


Figure 5: The reactive sensing principle. A molecule binding to the microsphere surface is polarized within the evanescent field (yellow ring) of the a WGM optical resonance. The energy that is needed to polarize the molecule causes the resonance frequency shift.

Evanescent field: Total internal reflection of light at a prism surface produces a non-propagating evanescent field that decays exponentially with distance from the reflecting surface. The evanescent field length extends typically a distance given by a fraction of the wavelength, or about 100–300 nm at visible wavelengths.

Polarizability: The polarizability of a molecule describes the tendency of its charge distribution—given by the electron clouds around its atoms—to be distorted from an external electric or electromagnetic field.

the evanescent field generated in the sphere by TIR. Similar to the case of a prism, the **evanescent field** of a WGM extends about 300 nm into the surrounding aqueous medium. Once bound within this evanescent field, every atom of the Streptavidin molecule will become polarized (at optical frequency) and the overall induced dipole moment P in response to the electric field strength E is calculated as $P = \alpha \times E$, where α is the excess polarizability of Streptavidin. The energy that is needed to polarize the molecule and induce this dipole moment is calculated from $\hbar\omega = \frac{1}{2} \alpha |\vec{E}(\vec{r}_0)|^2$,

where E is the electric field strength at the Streptavidin binding site r_0 . Note that we are working in aqueous solution and have to consider the *excess* polarizability α , here $\alpha_{\text{Streptavidin}} = 4\pi\epsilon_0 \times 3.3 \times 10^{-21} \text{ cm}^3$, in excess to the displaced water solution.²³ By first order perturbation theory, we can now estimate the frequency shift by comparing the energy quanta that is needed to polarize the biomolecule to the total electromagnetic field energy stored in the resonator:¹⁵

$$\frac{\Delta\omega}{\omega} = - \frac{\alpha |\vec{E}(\vec{r}_0)|^2}{2 \int \epsilon |\vec{E}'(\vec{r})|^2 dV} \quad (4)$$

where $\epsilon = \epsilon_\rho \epsilon_0$ is the permittivity of the resonator medium which here is glass. The reactive sensing principle applies to any microcavity and to any biomolecule and allows researchers to quantify the frequency shift of any optical resonator biosensor in response to molecular or nanoparticle binding events.

2.3 Detecting molecular mass loading

For the case of molecules bound at random locations on the microsphere cavity, we can integrate equation (4) over the complete resonator surface and obtain:

$$\frac{\Delta\omega}{\omega} = - \frac{\sigma\alpha}{\epsilon_0(n_s^2 - n_m^2)R} \quad (5)$$

where σ is the surface density of bound proteins (in units cm^{-2}). Applied to the microsphere of radius R , equation (5) allows us to calculate the surface density of a bound protein for any given time from the measured change in resonance frequency $\frac{\Delta\omega}{\omega}$, where n_s is the refractive index of the microsphere and n_m is the refractive index of the surrounding solution, here water with $n = 1.33$. The only unknown molecular parameter is the

excess polarizability α which scales proportional to the molecular weight of a given biopolymer such as protein or DNA. The excess polarizability for protein or DNA biopolymer is determined from measurements of the refractive index increment dn/dc of the pure biopolymer solution. The excess polarizability is then related to the refractive index increment by

$$\alpha = \epsilon_0 2n_m \left(\frac{dn}{dc} \right)_{biopolymer} m_{biopolymer} \quad (6)$$

where ϵ_0 is the vacuum permittivity, n_m is the solvent refractive index (water), m is the molecular weight of the biopolymer (Streptavidin: $\sim 1 \times 10^{-19}$ gram) and dn/dc of protein¹⁴ is ~ 0.183 cm³/g, dn/dc of DNA ~ 0.166 cm³/g. With this equation (6) in hand, we can calculate the mass loading associated with the resonance frequency shift and plot the sensor response (**sensogram**) in units of mass loading:¹²

$$\text{mass.l.} \left[\frac{\text{pg}}{\text{mm}^2} \right] = - \frac{\Delta \varpi}{\varpi} \frac{(n_s^2 - n_m^2) \times R [\text{mm}]}{2 \times n_m \times \left(\frac{dn}{dc} \right)_{biopolymer} \left[\frac{\text{mm}^3}{\text{pg}} \right]} \quad (7)$$

Figure 6 shows the example of a WGM biosensor used for Fibronectin (FN) protein detection. Sensograms plotted in units of mass loading [ng/cm²] vs time [s] show FN protein adsorption for differently functionalized glass microspheres—one with hydrophobic 13F-coating and another one with hydrophilic polyethyleneglycol PEG-coating—from different solution concentration levels.³⁹ As expected, the amount of mass loading that is reached in equilibrium depends on the Fibronectin solution concentration level. By fitting of these results to a kinetic binding model such as the **Langmuir model** one can determine kinetic-on (k_{on}) and -off rates (k_{off}) as well as the dissociation constant $K_d = k_{\text{off}}/k_{\text{on}}$ which characterizes the affinity of the Fibronectin protein towards the particular microsphere coating 13F or PEG. Care has to be taken at higher solution concentration levels so that measurements are not affected by mass transport limitations.³⁹ Alternatively, the dissociation constant can be determined from a plot of surface coverage in equilibrium vs solution concentration level. Such a plot is called Langmuir isotherm and the dissociation constant K_d equals just the concentration level at which surface coverage is 50%.¹⁴ If the sensor surface is modified with specific recognition elements such as antibodies or antigens, the above analysis is used to determine the affinity of the recognition element towards the analyte. The above analysis establishes

the relationship between the sensor response—the amount or mass loading of specifically bound protein—and the protein solution concentration level. Once such sensor response has been experimentally determined or analytically calculated for different solution concentration levels, the sensor can then be used to determine the unknown concentration of the analyte molecule.¹⁴ It is important to note that the specific detection of an analyte or biomarker can only be achieved if the optical resonator biosensor is functionalized with specific biorecognition elements, such as an **antibody**, oligonucleotide, aptamer, etc. Table 3 gives an overview of the biorecognition elements, the detected biomarkers and the minimal solution concentration levels that have been identified.

2.4 Nanoparticle and single virus detection

We can also use the reactive sensing principle to predict the maximum frequency shift for the binding of a single nanoparticle to the equator of the microsphere. For this analysis, we have to take into account the radius of the nanoparticle a as well as the evanescent field length L :

$$\left(\frac{\Delta \varpi}{\varpi} \right)_{\text{max}} \cong -D \frac{a^3}{R^{5/2} \lambda^{1/2}} e^{-a/L} \quad (8)$$

with

$$D = 2n_m^2 (2n_s)^{1/2} (n_{\text{np}}^2 - n_m^2) / (n_s^2 - n_m^2) (n_{\text{np}}^2 + 2n_m^2)$$

$$L \approx (\lambda/4\pi) (n_s^2 - n_m^2)^{-1/2}$$

where n_{np} is the refractive index of the nanoparticle.¹⁰ This equation in conjunction with (6) has been used to extract the size and mass of a single **Influenza A virus** particle, from the discrete resonance frequency shifts that were observed upon binding of the virion to the equator of a $R = 30$ μm glass microsphere, with resonances excited at $\lambda \sim 763$ nm wavelength,¹⁰ see figure 7. The sizing of virions and nanoparticles with optical resonator biosensors is a fast growing area of research and recent demonstrations of the detection and sizing of nanoparticles down to few 10's of nanometer size range^{32,45,84} are rapidly approaching the single molecule detection limit, where a biomolecule has a radius of ~ 3 nm.

3 Optical Resonator Biomolecular Logic Devices

3.1 Bacteriorhodopsin molecular switches

Biological molecules can undergo **conformational changes** on optical excitation. A common feature of most of these molecules is the generation of a photocycle upon illumination with light. On

Antibody: An antibody is a protein with a characteristic Y-shaped structure that specifically binds to a target molecule called the antigen. Antibodies are produced by the B-cells of the immune system and are widely used in biosensor applications because of their ability to only recognize the target antigen even against a background of many other biomolecules in solution.

Sensogram: Plot of sensor response versus time.

Influenza A virus: Influenza A Virus is also called the flu virus. It causes the seasonal flu and mutations of the virus can trigger pandemics such as the Spanish flu which broke out in 1918.

Langmuir model: The Langmuir model describes the equilibrium between molecules in solution and their independent and fixed number of binding sites at the surface of a substrate such as a biosensor.

Conformational change: The change in the three-dimensional structure of a biomolecule is called a conformational change. On a molecular level, conformational changes are responsible for muscle movement, signal transductions, etc.

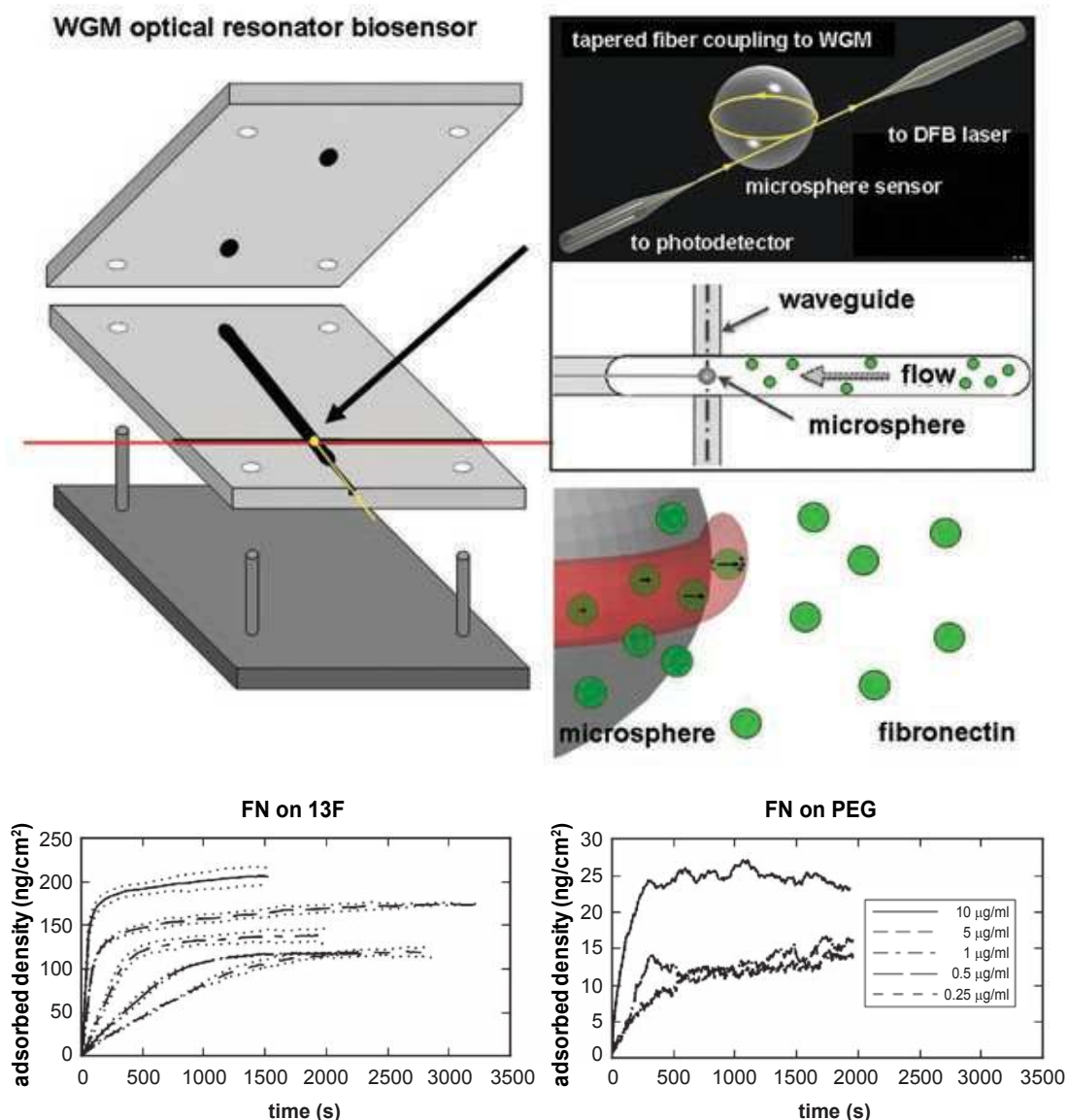


Figure 6: Top: WGM optical resonator biosensor integrated in flow cell. Resonance in a glass microsphere is excited via evanescent coupling from tapered fiber. Mass loading associated with binding of Fibronectin protein molecules (green) to the microsphere sensor surface is determined from WGM frequency shift, see also equation (7). Bottom, adapted from reference 39: Mass-loading sensograms for Fibronectin (FN) protein binding to differently modified glass microsphere surfaces functionalized with hydrophobic 13F (left) and hydrophilic PEG (right) coating. The sensogram in mass-loading versus time is determined for different solution concentration levels which here range from 10 $\mu\text{g/ml}$ to 0.25 $\mu\text{g/ml}$.

absorbing light, these molecules undergo conformational transitions that result in the formation of intermediate molecular species which finally relax back to the initial state. Figure 8 shows the photocycle of a particularly interesting photosensitive molecule called Bacteriorhodopsin that is found in the purple membrane fragments of *Halobacterium halobium*.

Bacteriorhodopsin has emerged as an outstanding photonic material for practical applications due

to its multifunctional photoresponse and unique properties. It exhibits high quantum efficiency of converting light into a state change, robustness to degeneration by environmental perturbations, response in the visible spectrum, low production cost and flexibility to tune its kinetic and spectral properties by genetic engineering techniques. It has been experimentally demonstrated that Bacteriorhodopsin can undergo more than a million switching cycles without getting denatured, an

Table 3: Overview of biomarkers that have been detected using recognition elements immobilized on the resonator surface. The minimal detectable mass loading and concentration levels are indicated. In some experiments mass loading was not reported separately.

Biomarker, approx. MW in kD	Optical resonator type	Recognition element	Approx. mass loading sensitivity	Approx. solution concentration sensitivity
Streptavidin ^{23,30} 56 kD	Glass microsphere	Biotin	1 pg/mm ²	1 nM
Fibronectin ³⁹ 440 kD	Glass microsphere	none	1–10 pg/mm ²	1–10 pM
Glucose oxidase 160 kD (manuscript in prep)	Glass microsphere	none	1–10 pg/mm ²	1 nM
Bacteriorhodopsin ⁷⁷ 26 kD	Glass microsphere	none	1 pg/mm ²	n/a
HER2 ⁵⁸ 138 kD	Glass capillary (LCORR)	HER2 antibody	n/a	0.1 nM
DNA ⁷⁸ 5–10 kD	Glass capillary (LCORR)	DNA	6 pg/mm ²	1 nM
Methylated DNA ⁵⁸ 5–10 kD	Glass capillary (LCORR)	methyl binding protein	n/a	1 nM
PSA ⁷⁹ 28 kD	Silicon ring resonator	antibody	n/a	0.4 nM
Interleukin 2,4,5 ^{80–81} 15 kD, 15 kD, 43 kD	Silicon ring resonator	antibody	n/a	6–100 pM
TNF ⁸⁰ 51 kD	Silicon ring resonator	antibody	n/a	100 pM
microRNA ^{82–83} 5–10 kD	Silicon ring resonator	antibody-DNA duplex, DNA	n/a	10 pM
Influenza A virus ^{10,32,45} 300 000 kD	Glass microsphere, glass toroid	none	170 attogram	1 fM

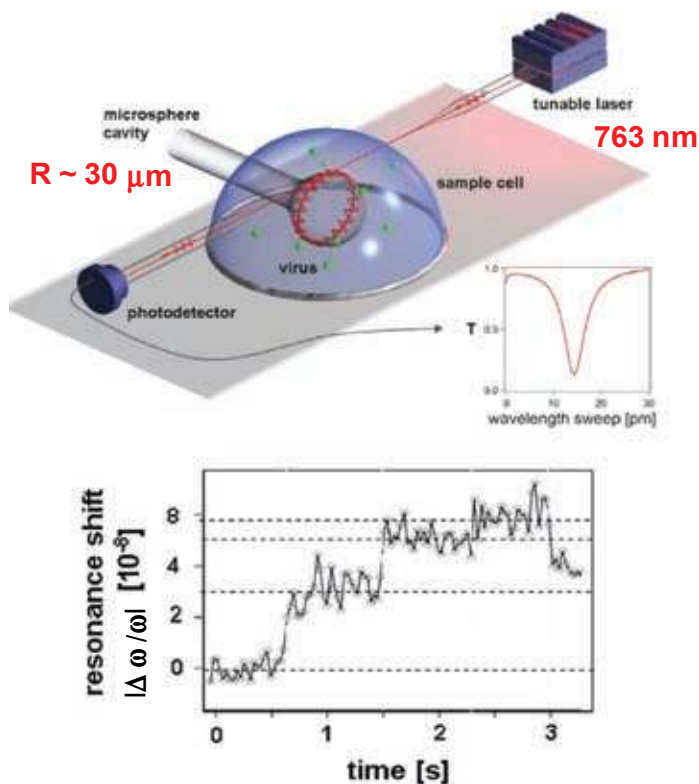


Figure 7: Top: Optical resonator biosensor setup for detection of single virus particles in a droplet of fluid, adapted from reference 10. An optical resonance (WGM) is excited with a DFB tunable laser diode at ~763 nm wavelength in ~60 μm diameter glass microsphere. Bottom: WGM frequency shifts recorded for the binding of single Influenza A virus particles.

Kramers-Kronig:
Special case of the Hilbert Transform which relates the real and imaginary parts of the refractive index.

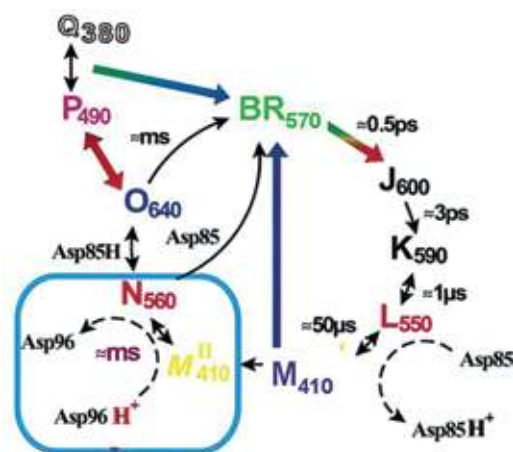


Figure 8: Photocycle of Bacteriorhodopsin with peak absorption wavelengths of intermediates indicated in subscripts.⁷²

astonishingly high level of reversibility. In addition, leophilized-dried Bacteriorhodopsin purple membrane preparations have no storage limit and Bacteriorhodopsin can retain its folded native structure up to temperatures as high as 140°C. These exceptional properties are attributed to the fact that it survives in extremely harsh conditions and has been optimized over centuries of evolution. Moreover, its 2D crystalline structure causes substantial stability towards thermal and chemical degradation.⁷²

A wide range of applications has been proposed for Bacteriorhodopsin.⁸⁵ Its proton pumping and photoelectric properties have been used for instance in desalination of sea water, conversion of sunlight to electricity, ultrafast light detection, chemo- and biosensing and artificial retinas. Its unique photochromic property has resulted in applications that include pattern recognition systems, associative and three-dimensional (3-D) memories, holography, and more recently even slow and fast light.⁸⁶ Table 4 summarizes the amazing optical properties of Bacteriorhodopsin in comparison to another important but synthetic organic photochromic molecule called diarylethene.

By absorbing green–yellow light, the Bacteriorhodopsin molecule undergoes several conformational transformations within a complex photocycle that sequentially generates a number of intermediate states. An important feature of all the intermediate states is their ability to be photochemically switched back to the initial-state by shining light at a wavelength that corresponds to the absorption peak of the intermediate in question.

Since the BR₅₇₀ and M₄₁₀ intermediates of the Bacteriorhodopsin molecule exhibit different absorption spectra, these molecules are called photochromes. Absorption spectroscopy is a convenient

means to monitor the molecular transformations of the Bacteriorhodopsin photocycle, and as pointed out before, light itself can be used to selectively and repeatedly switch Bacteriorhodopsin between the BR₅₇₀ and M₄₁₀ states, using green and blue light, respectively. We know from Kramers-Kronig transformation that any change in the absorption spectra of a molecule is also associated with a change in the polarizability (and related refractive index). Optical resonator biosensors are highly sensitive tools to monitor such polarizability changes, as any conformational change of surface-bound photochromic molecules will slightly change the path length and shift the resonance frequency.⁷⁷ In fact, microsphere optical cavities coated with Bacteriorhodopsin monolayers have been used to monitor the switching between BR₅₇₀ and M₄₁₀-states in real-time.⁸⁷ For this demonstration, the optical microcavity probed the Bacteriorhodopsin molecules with near-infrared WGMs so that the probing light could not trigger any conformational change. An external green and blue lightsource was then pointed on the microsphere to reversibly switch between BR₅₇₀ and M₄₁₀-state intermediates.^{75–76}

It is important to point out that Bacteriorhodopsin is structurally similar to the photoreceptor Rhodopsin in the human eye, see Figure 9. The Bacteriorhodopsin protein component, a seven alpha helix transmembrane protein, chaperons the photosensitive component called retinal (or Vitamin A) caged within the protein's hydrophobic center. Bacteriorhodopsin photoresponse cannot occur if Vitamin A is missing, so does lack of Vitamin A in the human photoreceptor Rhodopsin due to malnutrition, leads to a symptom called night-blindness.

Bacteriorhodopsin can be immobilized on the optical resonator microsphere surface using layer-by-layer deposition⁷⁷ where it forms a highly oriented monolayer consisting of oriented protein and Retinal components. By investigating the optical resonance frequency shifts associated with the photocycle of Bacteriorhodopsin it is possible to investigate the molecular transformations and it can be shown that the conformational change upon absorption of light is entirely due to a change in the molecular structure of Retinal, also known as *cis-trans* isomerisation.⁷⁷ In the BR₅₇₀-state, Retinal absorbs green light and this energy is used to 'flip' the retinal carbon-carbon double bond number 13 from the *trans* to the *cis* configuration of the M₄₁₀-state, see Figure 9 bottom.

According to the analytical result of the reactive sensing principle, equation 5, the frequency shift of a microsphere resonance upon Retinal isomerization is proportional to the change of

Table 4: Properties of Bacteriorhodopsin and Diarylethene photochromes.		
Property	Bacteriorhodopsin ⁸⁵	Diarylethene ⁸⁸⁻⁸⁹
Spectral range	400–700 nm	300–700 nm open ring isomers : 230–460 nm closed ring isomers: 425–830 nm
Quantum efficiency	64% B → K	50% between unconjugated open-ring isomer and conjugated closed-ring isomer quantum yields 0.01 to 0.86
Optical density	1–5 (at 570 nm)	0.5–0.72 (at 633 nm)
Maximal bleaching ratio	95%	
Refractive index	1.47 at 570 nm	1.533 at 785 nm
Refractive index change	0.001–0.01 (depends on OD)	$4 \times 10^{-2} - 1.5 \times 10^{-4}$
Diffraction efficiency	1–3%, max. 7%	1.2%
Light sensitivity	0.1–20 mJ/cm ²	
Reversibility	10 ⁶ cycles	10 ⁴ cycles normally 10 ⁶ cycles using the super low power laser irradiance
Shelf life	years	years
Film thickness	~10 nm–500 μm	300 nm
Aperture	unlimited	0.55
Stability of films Exposure to sunlight in the presence of air/oxygen	years	
Thermal stability	over 80°C (in water) and up to 140°C (dry)	open- and closed-ring isomers stable at 80°C
Chemical stability	pH values from 0 to 12	
Ionic strength	high ~3 M NaCl digestion by most proteases	

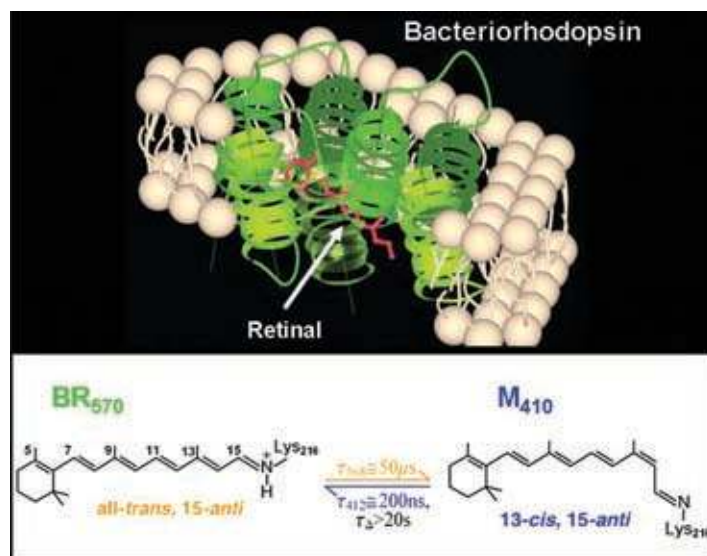


Figure 9: Top: Bacteriorhodopsin, composed of protein (green) within a lipid bilayer (white) chaperoning Retinal (red) at its center. Bottom: Conformational change of Retinal: cis-trans isomerization. Optical switching speeds are indicated, thermal equilibration takes about 20 seconds.

molecular polarizability and the surface density of the bound Retinal molecules. With the Retinal surface density in the monolayer coating at $9.12 \times 10^{12} \text{ cm}^{-2}$ and the photoinduced polarizability change ($\Delta\alpha$) associated with retinal isomerization measured at several hundreds of atomic units per Retinal molecule, high-Q ($Q \geq 10^5$) silica microspheres are exceptionally sensitive to $\Delta\alpha$ even in ultra-thin 4.5 nm Bacteriorhodopsin monolayers. In fact the conformational change of a single Retinal monolayer tunes the microsphere resonator entirely from off to on resonance, shifting the resonance line through more than one line width. The ability to tune the Bacteriorhodopsin-coated cavity completely from off to on resonance using visible green and blue control lights can be used to construct all-optical switches, routers and logic devices.

3.2 All-optical Bacteriorhodopsin-coated microresonator switches

A microsphere resonator coated with a Bacteriorhodopsin monolayer and connected to two optical fibers is a device that can be used to switch and re-route near infrared light (1310/1550 nm), Figure 10 (a). The configuration consists of two input and two output ports (1–4) located at the four fiber ends.

By coating the microsphere cavity with a photostable photochrome such as Bacteriorhodopsin, it is possible to demonstrate switching of near-infrared light using visible green and blue control lights to reversibly tune the cavity from off to on resonance. Figure 10 shows the operation principle:⁹⁰ switched on-resonance, near infrared light entering from port 1 can be almost completely rerouted to output port 3, whereas off-resonance near infrared light entering from port 1 will exit at port 2. The switch is actuated using a low-power green control beam that tunes the Bacteriorhodopsin coated cavity on resonance. Figure 11 shows the temporal response of the switch by reversibly applying the green and blue control lights.

3.3 All-optical Bacteriorhodopsin-coated microresonator logic gates and circuits

The major challenge in the practical realization of optical logic has so far been in meeting essential requirements of cascability, fan-out, logic-level restoration, input-output isolation, absence of critical level biasing, logic level independent of loss, and of course, low-power operation. The advantages of both Bacteriorhodopsin based microcavity

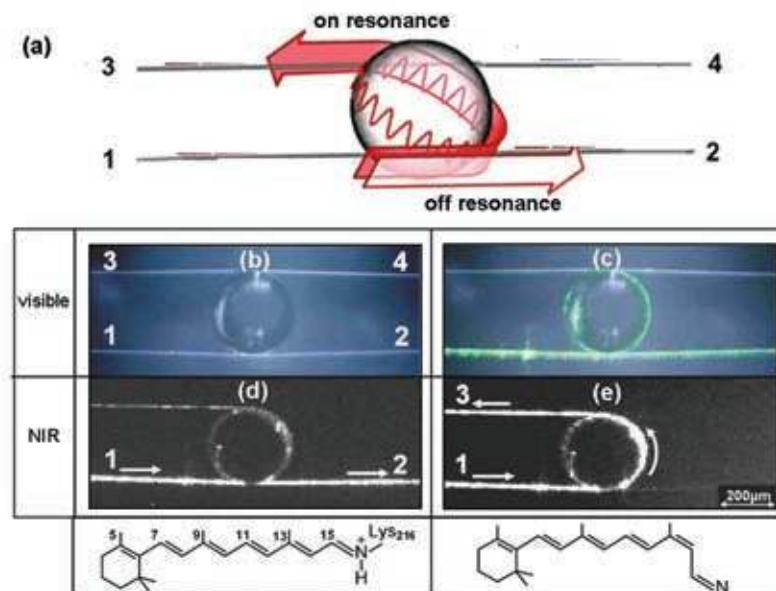


Figure 10: (a) Schematic of a Bacteriorhodopsin coated microsphere resonator connected to two tapered optical fibers forming a four-port device, adapted from reference 87; (b) Top-view photomicrograph of a Bacteriorhodopsin-coated microsphere positioned between two tapered fibers. The image was obtained at ambient illumination with a CCD camera; (c) The same microsphere with a green control beam coupled to the resonator; (d) Image of the propagation of near-infrared light off resonance; (e) Near-infrared beam propagation when cavity is tuned on resonance by applying green light. The corresponding conformation states of the Retinal are shown below the photomicrographs.

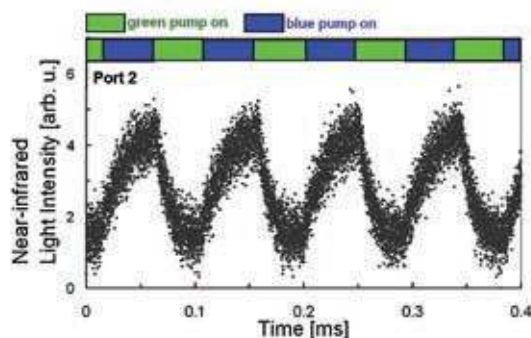


Figure 11: Switching operation of the 4-port Bacteriorhodopsin coated microsphere resonator, adapted from reference 25.

switch and tree architecture can be combined to design low-power all-optical computing circuits potentially meeting such requirements.^{25,90–92}

Conventional classical computing is based on Boolean logic that is irreversible, that is, the inputs cannot be inferred from the output, as the number of output bits is less than the inputs. This leads to destruction of information and hence to the dissipation of a large amount of energy. In contrast, conservative and reversible logic that can be achieved with Bacteriorhodopsin-coated microcavities (Fig. 10(a)), circumvents this problem by having equal number of inputs and outputs and opening up the possibility of ultra-low power computing. It is also compatible with revolutionary optical and quantum computing paradigms. A universal conservative and reversible logic gate is the Fredkin gate. The basic Fredkin Gate is a controlled swap gate that maps three inputs (C_{in} , I_1 , I_2) onto three outputs (C_{out} , O_1 , O_2). The C_{in} input is mapped directly to the C_{out} output, i.e., $C_{in} = C_{out}$. If $C = 0$, no swap is performed; I_1 maps to O_1 , and I_2 maps to O_2 . Otherwise, the two inputs are swapped, so that I_1 maps to O_2 , and I_2 maps to O_1 , as shown in the Table in Figure 12.⁹² It is easy to see that this circuit is reversible. The Fredkin Gate is the reversible 3-bit gate that swaps the last two bits if the first bit is 1 and can realize various other Boolean logic gates and circuits. It is interesting to note that a simple, single Bacteriorhodopsin-coated microcavity switch configuration considering the intensities of near-infrared signals and the green pump control signal, as the three inputs and outputs, realizes the important all-optical Fredkin gate.⁹¹

Many other reversible logic gates that include the Feynman, Feynman-double, Toffoli and Peres logic gates can be efficiently designed with optically controlled microresonators.⁹⁰ The most versatile combinatorial logic circuit is that of the Multiplexer (MUX) that can yield various kinds of

logic operations. Multiplexers and De-multiplexers (De-MUX) are also integral components of optical signal processing systems. A design of an all-optical MUX is as shown in figure 13, using three optically controlled microcavities.²⁵ The same circuit can be used to perform De-MUX operation with the select lines controlling the signal from a laser at OP to arrive at output ports IP1–4.

This basic switching configuration has been used to design a variety of other all-optical computing circuits, namely, half and full-adder/subtractor, full-adder avoiding fan-out and arithmetic unit.^{91–92} It is more advantageous to design a general circuit which has the capability to reconfigure and realize different arithmetic and logic operations. Bacteriorhodopsin-coated microcavity switches in tree architecture can also be used to realize reconfigurable all-optical logic and arithmetic operations.⁹⁰ Designing circuits based on Bacteriorhodopsin-coated microcavity as a template would require cascading these switches and converting optical signals between the visible and near infrared and vice-versa. These wavelength converters would limit compactness, low-power and speed of operation. However, judicious designs can avoid their use as shown for designing a wide range of computing circuits.^{25,90–92}

4 Outlook: Optical Resonator Based Sensing and Computation with Biomolecules

Optical resonator biosensors are emerging as one of the most sensitive microsystems biodetection technology that does not require amplification or labeling of the biomarker. The label-free optical resonator biosensor platform is highly versatile and future implementations will be tailored to specific detection needs for example in the life sciences, in environmental monitoring and in healthcare. We envision that clinical diagnostic assays—currently performed by trained medical personnel in well-equipped clinical laboratories—will be replaced by inexpensive and portable chip-scale optical resonator biosensor devices that can be operated in low-resource settings and by untrained personnel. To achieve this goal it will be particularly important to overcome challenges associated with integrating multiplexed optical resonator biosensors with other microfluidic, photonic and electronic components. First successfully integrated prototypes are already being tested in the commercial world (Genalyte Inc., Nanobioanalytics)^{24,53} and we expect many more to follow.

Several physical mechanisms have been proposed to boost sensitivity of optical resonator biosensors towards achieving the ultimate goal of

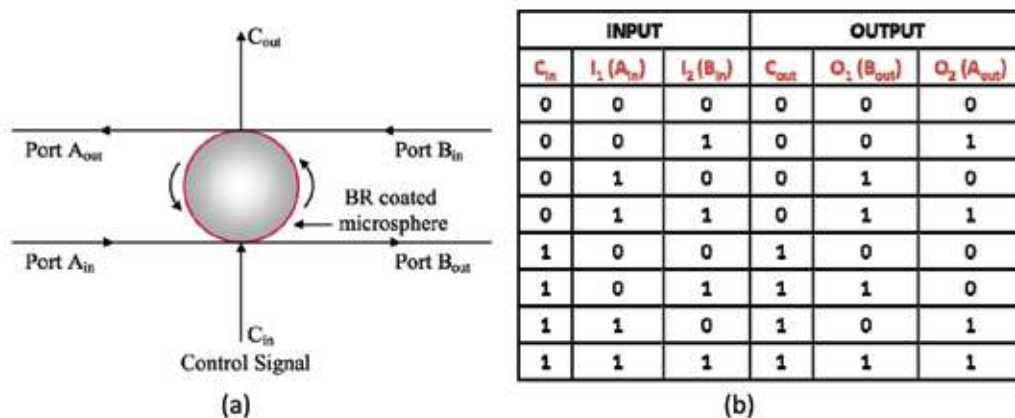


Figure 12: (a) Schematic of an all-optical universal Fredkin logic gate; (b) Truth table. BR = Bacteriorhodopsin. Adapted from reference 91.

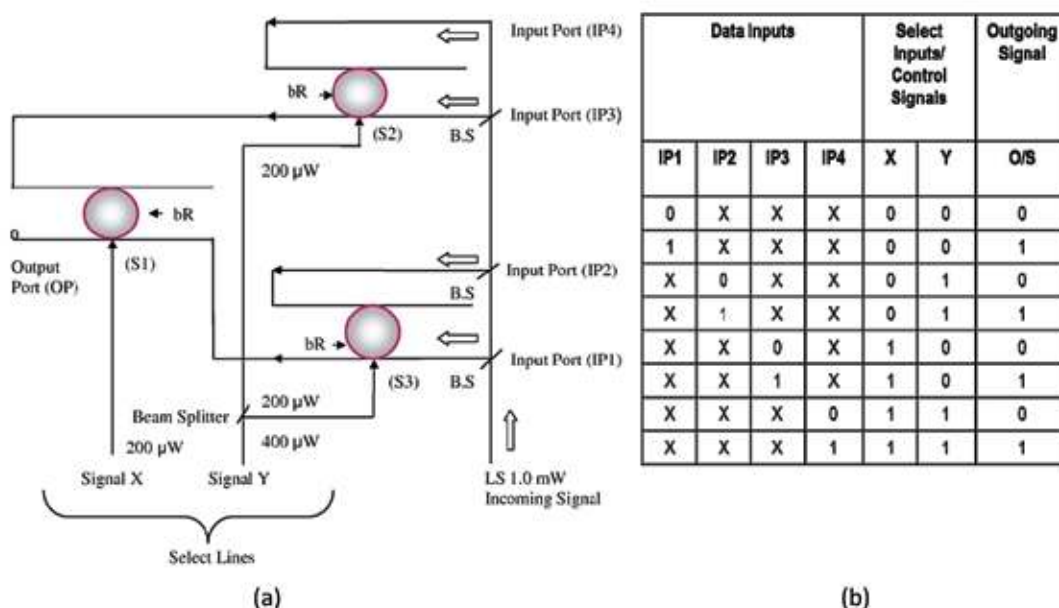


Figure 13: (a) Design of an all-optical multiplexer (MUX) with three Bacteriorhodopsin (bR)—coated microcavities; (b) Truth table. Adapted from reference 25.

label-free single molecule detection¹² which would revolutionize molecular diagnostics as well as provide for a deeper understanding of the biomolecular world, their self-assembly, functions and interactions. A particularly promising approach towards achieving this goal is based on the use of plasmonic nanoantennas for enhancing the frequency shift signal⁷⁵ and we refer to other¹² as well as future reviews on this emerging topic.

The detailed analysis of the optical response of biomaterials such as Bacteriorhodopsin is another promising research direction that leverages optical resonators for gaining novel insights with relevance to the burgeoning area of energy science.

For example, detailed understanding of energy conversion in photosynthetic systems and their quantitative analysis with optical resonator biosensors may lead to a better fundamental understanding, optimization and application of green energy resources.

Optical resonators also provide a highly sensitive interface for monitoring the functionality of photosensitive biomolecules which can be used to perform all-optical switching and logic operations. All-optical computation is a very active research area and usually the domain of atomic- and quantum optics. Microresonators functionalized with Bacteriorhodopsin may provide a complementary approach

to these established domains with particularly interesting science that may come out of switching single molecules with single photons. Microresonators functionalized with Bacteriorhodopsin or other biomaterials also offer the possibility of using 2-D/3-D integrated architectures to form circuits and networks with extremely low-power budget. By integrating microresonators for optical computation and biosensing in one simple platform one can envision all-optical devices that perform several biosensing assays, acquire, process, transmit and even store information and then optically display the results of a multiplexed measurement.

Received 1 March 2012.

References

- J. L. Arlett, E. B. Myers and M. L. Roukes, *Nat. Nanotechnol.* **6** (4), 203–215 (2011).
- P. S. Waggoner and H. G. Craighead, *Lab Chip* **7** (10), 1238–1255 (2007).
- F. Patolsky, G. Zheng and C. M. Lieber, *Nanomedicine* **1** (1), 51–65 (2006).
- J. Li, Y. J. Lu, Q. Ye, M. Cinke, J. Han and M. Meyyappan, *Nano Lett.* **3** (7), 929–933 (2003).
- F. Vollmer and S. Arnold, *Nature Methods* **5** (7), 591–596 (2008).
- P. Alivisatos, *Nat. Biotechnol.* **22** (1), 47–52 (2004).
- J. N. Anker, W. P. Hall, O. Lyandres, N. C. Shah, J. Zhao and R. P. Van Duyne, *Nat. Mater.* **7** (6), 442–453 (2008).
- K. K. Jain, *Clin. Chim. Acta* **358** (1–2), 37–54 (2005).
- G. M. Whitesides, *Nat. Biotechnol.* **21** (10), 1161–1165 (2003).
- F. Vollmer, S. Arnold and D. Keng, *Proc. Natl. Acad. Sci. U.S.A.* **105** (52), 20701–20704 (2008).
- A. K. Naik, M. S. Hanay, W. K. Hiebert, X. L. Feng and M. L. Roukes, *Nat. Nanotechnol.* **4** (7), 445–450 (2009).
- M. Baaske and F. Vollmer, *ChemPhysChem* **13** (2), 427–436 (2012).
- F. Patolsky, G. F. Zheng, O. Hayden, M. Lakadamyali, X. W. Zhuang and C. M. Lieber, *Proc. Natl. Acad. Sci. U.S.A.* **101** (39), 14017–14022 (2004).
- K. Wilson and F. Vollmer, *Encyclopedia of Nanotechnology* **in press** (2012).
- S. Arnold, M. Khoshshima, I. Teraoka, S. Holler and F. Vollmer, *Opt. Lett.* **28** (4), 272–274 (2003).
- T. P. Burg, M. Godin, S. M. Knudsen, W. Shen, G. Carlson, J. S. Foster, K. Babcock and S. R. Manalis, *Nature* **446** (7139), 1066–1069 (2007).
- F. Patolsky, G. F. Zheng and C. M. Lieber, *Nat. Protoc.* **1** (4), 1711–1724 (2006).
- H. K. Hunt, C. Soteropulos and A. M. Armani, *Sensors* **10** (10), 9317–9336 (2010).
- M. Curreli, R. Zhang, F. N. Ishikawa, H. K. Chang, R. J. Cote, C. Zhou and M. E. Thompson, *IEEE Trans. Nanotechnol.* **7** (6), 651–667 (2008).
- B. Ilic, Y. Yang and H. G. Craighead, *Appl. Phys. Lett.* **85** (13), 2604–2606 (2004).
- X. D. Fan and I. M. White, *Nat. Photonics* **5** (10), 591–597 (2011).
- A. J. Qavi, A. L. Washburn, J. Y. Byeon and R. C. Bailey, *Anal. Bioanal. Chem.* **394** (1), 121–135 (2009).
- F. Vollmer, D. Braun, A. Libchaber, M. Khoshshima, I. Teraoka and S. Arnold, *Appl. Phys. Lett.* **80** (21), 4057–4059 (2002).
- M. Iqbal, M. A. Gleeson, B. Spaugh, F. Tybor, W. G. Gunn, M. Hochberg, T. Baehr-Jones, R. C. Bailey and L. C. Gunn, *IEEE J. Sel. Top. Quantum Electron.* **16** (3), 654–661 (2010).
- S. Roy, M. Prasad, J. Topolancik and F. Vollmer, *J. Appl. Phys.* **107** (5), 053115–053115-9 (2010).
- D. N. Guerra, A. R. Bulsara, W. L. Ditto, S. Sinha, K. Murali and P. Mohanty, *Nano Lett.* **10** (4), 1168–1171 (2010).
- Y. Huang, X. F. Duan, Y. Cui, L. J. Lauhon, K. H. Kim and C. M. Lieber, *Science* **294** (5545), 1313–1317 (2001).
- F. Vollmer, PhD Thesis, Rockefeller University (2004).
- V. S. Ilchenko and A. B. Matsko, *IEEE J. Sel. Top. Quantum Electron.* **12** (1), 15–32 (2006).
- C. E. Soteropulos, H. K. Hunt and A. M. Armani, *Appl. Phys. Lett.* **99** (10), 9317–9336 (2011).
- L. N. He, S. K. Ozdemir, J. G. Zhu and L. Yang, *Physical Review A* **82** (5), 053810–053810-4 (2010).
- T. Lu, H. Lee, T. Chen, S. Herchak, J. H. Kim, S. E. Fraser, R. C. Flagan and K. Vahala, *Proc. Natl. Acad. Sci. U.S.A.* **108** (15), 5976–5979 (2011).
- I. M. White, H. Oveys and X. Fan, *Opt. Lett.* **31** (9), 1319–1321 (2006).
- Q. Quan, F. Vollmer, I. B. Burgess, P. B. Deotare, I. Frank, S. Tang, R. Illic and M. Loncar, 2011 (unpublished).
- M. Lee and P. M. Fauchet, *Opt. Express* **15** (8), 4530–4535 (2007).
- S. Mandal, J. M. Goddard and D. Erickson, *Lab Chip* **9** (20), 2924–2932 (2009).
- J. Lutti, W. Langbein and P. Borri, *Appl. Phys. Lett.* **93** (15), 151103–151103-3 (2008).
- H. Y. Zhu, I. M. White, J. D. Suter, M. Zourob and X. D. Fan, *Anal. Chem.* **79** (3), 930–937 (2007).
- K. A. Wilson, C. A. Finch, P. Anderson, F. Vollmer and J. J. Hickman, *Biomaterials* **33** (1), 225–236 (2012).
- N. M. Hanumegowda, C. J. Stica, B. C. Patel, I. White and X. D. Fan, *Appl. Phys. Lett.* **87** (20), 201107–201107-3 (2005).
- I. Teraoka and S. Arnold, *J. Opt. Soc. Am. B-Opt. Phys.* **23** (7), 1434–1441 (2006).
- H. C. Ren, F. Vollmer, S. Arnold and A. Libchaber, *Opt. Express* **15** (25), 17410–17423 (2007).
- S. Arnold, D. Keng, S. I. Shopova, S. Holler, W. Zurawsky and F. Vollmer, *Opt. Express* **17** (8), 6230–6238 (2009).
- V. S. Ilchenko, X. S. Yao and L. Maleki, *Opt. Lett.* **24** (11), 723–725 (1999).
- L. He, S. K. Ozdemir, J. Zhu, W. Kim and L. Yang, *Nat Nano* **6** (7), 428–432 (2011).
- A. Yalcin, K. C. Popat, J. C. Aldridge, T. A. Desai, J. Hryniewicz, N. Chbouki, B. E. Little, O. King, V. Van,

- S. Chu, D. Gill, M. Anthes-Washburn and M. S. Unlu, *IEEE J. Sel. Top. Quantum Electron.* **12** (1), 148–155 (2006).
47. C. Y. Chao, W. Fung and L. J. Guo, *IEEE J. Sel. Top. Quantum Electron.* **12** (1), 134–142 (2006).
48. A. Ksendzov and Y. Lin, *Opt. Lett.* **30** (24), 3344–3346 (2005).
49. C. Delezoide, M. Salsac, J. Lautru, H. Leh, C. Nogues, J. Zyss, M. Buckle, I. Ledoux-Rak and C. T. Nguyen, *IEEE Photonics Technol. Lett.* **24** (4), 270–272 (2012).
50. A. Ramachandran, S. Wang, J. Clarke, S. J. Ja, D. Goad, L. Wald, E. M. Flood, E. Knobbe, J. V. Hryniewicz, S. T. Chu, D. Gill, W. Chen, O. King and B. E. Little, *Biosens. Bioelectron.* **23** (7), 939–944 (2008).
51. J. T. Kirk, G. E. Fridley, J. W. Chamberlain, E. D. Christensen, M. Hochberg and D. M. Ratner, *Lab Chip* **11** (7), 1372–1377 (2011).
52. A. Francois and M. Himmelhaus, *Appl. Phys. Lett.* **94** (3), 031101–031101-3 (2009).
53. M. Himmelhaus, S. Krishnamoorthy and A. Francois, *Sensors* **10** (6), 6257–6274 (2010).
54. M. Himmelhaus and A. Francois, *Biosens. Bioelectron.* **25** (2), 418–427 (2009).
55. J. Yang and L. J. Guo, *IEEE J. Sel. Top. Quantum Electron.* **12** (1), 143–147 (2006).
56. A. Weller, F. C. Liu, R. Dahint and M. Himmelhaus, *Appl. Phys. B-Lasers Opt.* **90** (3–4), 561–567 (2008).
57. E. Nuhiji and P. Mulvaney, *Small* **3** (8), 1408–1414 (2007).
58. J. T. Gohring, P. S. Dale and X. D. Fan, *Sens. Actuator B-Chem.* **146** (1), 226–230 (2010).
59. A. Schweinsberg, S. Hocde, N. N. Lepeshkin, R. W. Boyd, C. Chase and J. E. Fajardo, *Sens. Actuator B-Chem.* **123** (2), 727–732 (2007).
60. R. W. Boyd and J. E. Heebner, *Appl. Optics* **40** (31), 5742–5747 (2001).
61. M. Pollinger, D. O’Shea, F. Warken and A. Rauschenbeutel, *Phys. Rev. Lett.* **103** (5), 053901–053901-4 (2009).
62. E. J. Smith, S. Schulze, S. Kiravittaya, Y. F. Mei, S. Sanchez and O. G. Schmidt, *Nano Lett.* **11** (10), 4037–4042 (2011).
63. I. D. Block, L. L. Chan and B. T. Cunningham, *Sens. Actuator B-Chem.* **120** (1), 187–193 (2006).
64. D. Erickson, S. Mandal, A. H. J. Yang and B. Cordovez, *Microfluid. Nanofluid.* **4** (1–2), 33–52 (2008).
65. D. A. Bergstein, E. Ozkumur, A. C. Wu, A. Yalcin, J. R. Colson, J. W. Needham, R. J. Irani, J. M. Gershoni, B. B. Goldberg, C. DeLisi, M. F. Ruane and M. S. Unlu, *IEEE J. Sel. Top. Quantum Electron.* **14** (1), 131–139 (2008).
66. M. Trupke, E. A. Hinds, S. Eriksson, E. A. Curtis, Z. Muktadir, E. Kukharenska and M. Kraft, *Appl. Phys. Lett.* **87** (21) (2005).
67. F. Vollmer and P. Fischer, *Opt. Lett.* **31** (4), 453–455 (2006).
68. A. Watkins, J. Ward, Y. Q. Wu and S. N. Chormaic, *Opt. Lett.* **36** (11), 2113–2115 (2011).
69. R. Henze, T. Seifert, J. Ward and O. Benson, *Opt. Lett.* **36** (23), 4536–4538 (2011).
70. M. Sumetsky, Y. Dulashko and R. S. Windeler, *Opt. Lett.* **35** (7), 898–900 (2010).
71. J. Scheuer and M. Sumetsky, *Laser Photon. Rev.* **5** (4), 465–478 (2011).
72. M. Sumetsky, *Opt. Express* **12** (10), 2303–2316 (2004).
73. F. Xu, P. Horak and G. Brambilla, *Opt. Express* **15** (12), 7888–7893 (2007).
74. J. D. Swaim, J. Knittel and W. P. Bowen, *Appl. Phys. Lett.* **99** (24), 243109–243109-3 (2011).
75. M. A. Santiago-Cordoba, S. V. Boriskina, F. Vollmer, and M. C. Demirel, *Applied Physics Letters* **99** (7), 073701–073701-3 (2011).
76. S. I. Shopova, R. Rajmangal, S. Holler and S. Arnold, *Appl. Phys. Lett.* **98** (24) (2011).
77. J. Topolancik and F. Vollmer, *Biophys. J.* **92** (6), 2223–2229 (2007).
78. F. Vollmer, S. Arnold, D. Braun, I. Teraoka and A. Libchaber, *Biophys. J.* **85** (3), 1974–1979 (2003).
79. A. L. Washburn, J. Gomez and R. C. Bailey, *Anal. Chem.* **83** (9), 3572–3580 (2011).
80. M. S. Luchansky and R. C. Bailey, *J. Am. Chem. Soc.* **133** (50), 20500–20506 (2011).
81. M. S. Luchansky and R. C. Bailey, *Anal. Chem.* **82** (5), 1975–1981 (2010).
82. A. J. Qavi, J. T. Kindt, M. A. Gleeson and R. C. Bailey, *Anal. Chem.* **83** (15), 5949–5956 (2011).
83. A. J. Qavi and R. C. Bailey, *Angew. Chem.-Int. Edit.* **49** (27), 4608–4611 (2010).
84. J. G. Zhu, S. K. Ozdemir, Y. F. Xiao, L. Li, L. N. He, D. R. Chen and L. Yang, *Nat. Photonics* **4** (1), 46–49 (2010).
85. N. Hampp, *Chem. Rev.* **100** (5), 1755–1776 (2000).
86. P. F. Wu and D. Rao, *Phys. Rev. Lett.* **95** (25), 253601–253601-4 (2005).
87. J. Topolancik and F. Vollmer, *Appl. Phys. Lett.* **89** (18), 184103–184103-3 (2006).
88. M. Irie, *Chem. Rev.* **100**, 1685–1716 (2000).
89. S. Luo, K. Chen, L. Cao, G. Liu, Q. He and G. Jin, *Opt. Express* **13**, 3123–3128 (2005).
90. S. Roy, P. Sethi, J. Topolancik and F. Vollmer, *Adv. Opt. Technol.*, 727206–727201–727206–727212 (2012).
91. S. Roy and M. Prasad, *Opt. Eng.* **49** (6), 065201–1–065201-11 (2010).
92. S. Roy and M. Prasad, *IEEE Trans. Nanobiosci.* **10** (3), 160–171 (2011).



Dr. Frank Vollmer obtained his PhD from the 'Center for Studies in Physics and Biology' at the Rockefeller University NYC in 2004. He then became leader of an independent research group at the Rowland Institute at Harvard University where he was appointed Rowland Fellow from 2004 to 2009. From 2010–2011 he joined the Wyss Institute for Bio-Inspired Engineering at Harvard University as a Scholar-in-Residence. In 2011 he was appointed group leader of a Max Planck Research Group at the Max Planck Institute for the Science of Light in Erlangen, Germany. Dr. Vollmer also holds an external appointment as Associate Biologist and Instructor in Medicine (PI) at Brigham and Women's Hospital in Boston, USA. More information can be found on the Max Planck Research Group web site Laboratory of Biophotonics & Biosensing <http://mpl.mpg.de/mpf/php/bfp/index.html>



Dr. Sukhdev Roy obtained his PhD in Physics from the Indian Institute of Technology Delhi, in 1993 and joined the Department of Physics and Computer Science, Dayalbagh Educational Institute (Deemed University), Agra, where he is at present a Professor. He has been a Visiting Scientist at the Rowland Institute at Harvard University, University of Waterloo, Osaka University, Hokkaido University, City University, London, Queen Mary University of London, Tata Institute of Fundamental Research, Mumbai and the Indian Institute of Science, Bangalore. He is an Associate of the Abdus Salam International Centre for Theoretical Physics, Trieste, Italy. He has won a number of awards and fellowships that include the JSPS Invitation Fellowship, Japan, 2004, the 1st IETE B.B. Sen Memorial Award, 2007, Hari Om Ashram Prerit H.C. Shah Research Endowment Prize by Sardar Patel University, 2006, AICTE Career Award for Young Teachers, 2001 and many best paper awards. He was the Guest Editor of the March 2011 Special Issue of IET Circuits, Devices and Systems Journal (U.K.) on Optical Computing.

